

TECHNOLOGIES FOR MASS PRODUCTION OF > 20 % EFFICIENT P-TYPE SILICON SOLAR CELLS

S. Mack, A. Wolf, B. Thaidigsmann, E. Lohmüller, U. Jäger, M. Pospischil, F. Clement, D. Eberlein, R. Preu, D. Biro
Fraunhofer Institute for Solar Energy Systems ISE, Heidenhofstrasse 2, 79110 Freiburg, Germany
e-mail: sebastian.mack@ise.fraunhofer.de, phone: +49 761 4588 5580, fax: +49 761 4588 9250

ABSTRACT: This paper summarizes the results of the project “MASSE”, which focused on the research and development of technologies and process sequences for mass production of 20 % efficient monocrystalline p-type silicon solar cells. This goal is addressed by the use of PERC (passivated emitter and rear cell) and MWT-PERC (metal wrap through PERC) structures. Within the frame of the project, several technologies have been investigated in detail and optimised carefully. The various technologies are modular, which allows for an application both in PERC and MWT-PERC structures. We propose the use of thermal oxidation for simultaneous high quality front and rear surface passivation. On high-quality float-zone silicon, which we use for determining the efficiency potential of these structures, the best PERC solar cells achieve a conversion efficiency of 20.0 %; reduced shading in MWT-PERC type devices increases this value to 20.3 %. In both cases, screen printing forms the front and rear contacts. The implementation of dispensed silver front contacts in MWT-PERC structures increases the maximum cell efficiency even further to 20.6 %. Solder pads enable module assembly with existing equipment. By using rectangular masks for aperture area definition, conversion efficiencies of 17.7 % for PERC and 18.2 % for MWT-PERC modules are measured.

Keywords: thermal oxidation, SiO₂, passivation, MWT, PERC, HIP-MWT, silicon solar cell

1 INTRODUCTION

Recently, many research institutes, universities and R&D departments reported on progress in surface passivation and process sequences for the fabrication of high efficient p-type passivated emitter and rear cell (PERC) structures [1-4]. Due to the increased conversion efficiency, an industrial PERC device results in increased market attention and in the possibility for increased income with this premium product.

Compared to standard p-type H-pattern solar cells with an aluminum back surface field (Al-BSF), PERC type cells feature a dielectrically passivated rear surface with local contacts, whereas the front of the cell typically is identical. A different solar cell structure that addresses changes in the contact layout at the front is the metal wrap through (MWT) concept [5], in which the external busbar contacts are moved from the front to the rear, resulting in reduced shading.

Starting from a process sequence for the fabrication of PERC devices, the introduction of only one additional process step, namely via drilling, allows for combining MWT with PERC structures [6] and makes the full benefit of reduced shading accessible.

In this work, we report on the results of the project “MASSE”, which targeted the development of high-efficiency industrial p-type PERC and MWT-PERC solar cells and modules. Within the frame of the project, several technologies and fabrication sequences were tested.

In the following, the cell structures and technologies, which the authors have identified as most promising for an industrial realization, will be presented. All solar cells presented in this work feature thermal oxide passivation layers on both front and rear, and screen printed solder pads. For brevity, mainly the best results on high-quality float-zone silicon will be presented.

2 APPROACH

2.1 Fabrication of p-type PERC solar cells

Boron-doped float-zone silicon (FZ-Si) wafers with a base resistivity of 0.5 Ωcm and a thickness of 200 μm serve as starting material. Although the focus of the project is on mass production technologies, FZ-Si is used due to the absence of light induced degradation and the possibility of higher dopant concentration, as well as for determination of the efficiency potential of the developed cell structures.

The final cell structure is depicted in Fig. 1, the process flow in Fig. 2. After labelling, all samples are subject to random pyramid formation in alkaline KOH solution. The texture on the rear is removed by inline single side wet-chemical etching to allow for higher open circuit voltages [7], probably due to a lower interface trap density [8]. Due to process availability, instead of wet chemical edge isolation subsequent to atmospheric pressure POCl₃-diffusion, a SiO_x diffusion barrier is applied by plasma-enhanced chemical vapour deposition (PECVD) on the rear surface. After POCl₃-diffusion, a selective emitter is formed on the front by laser-overdoping from phosphosilicate glass (PSG), followed by PSG removal and a RCA clean.

Several dielectric layers are known to allow for low surface recombination velocities on p-type silicon, e.g. SiO₂, Al₂O₃, SiO_xN_y or SiN_x. In this work, we use thin SiO₂ layers fabricated by thermal oxidation in a high-capacity industrial tube furnace in oxygen ambient due to its low density of interface traps, which yields low surface recombination velocities on both p-type and n-type silicon [9].

The thermal oxidation process is implemented into the fabrication process of p-type PERC solar cells by simultaneously growing a thin high-quality SiO₂ passivation layer on both front emitter and rear base. Thus, the thermal oxide passivates all sides (TOPAS [7]). As the thermal oxidation process improves the emitter quality by lowering the phosphorous surface concentration in the field emitter to around $2 \cdot 10^{20} \text{ cm}^{-3}$, the selective emitter ensures a low specific contact resistance.

A PECVD SiN_x layer applied on the front ensures a low reflection, PECVD capping layers on the rear SiO_2 layer improve surface passivation and prevent alloying of the screen printed aluminium through the passivation layers during contact firing. Solder pad and front metallization consist of standard single step screen printing. After laser fired contact (LFC, [10]) formation on the rear, a forming gas anneal in a high-capacity inline furnace [11], which was developed within the frame of this project, completes the fabrication sequence.

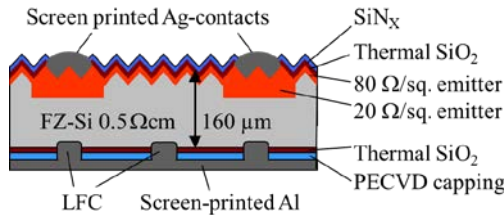


Fig. 1: Schematic cross section of the PERC-type cell discussed in this work with simultaneous front emitter and rear base passivation by a thin thermal oxide layer.

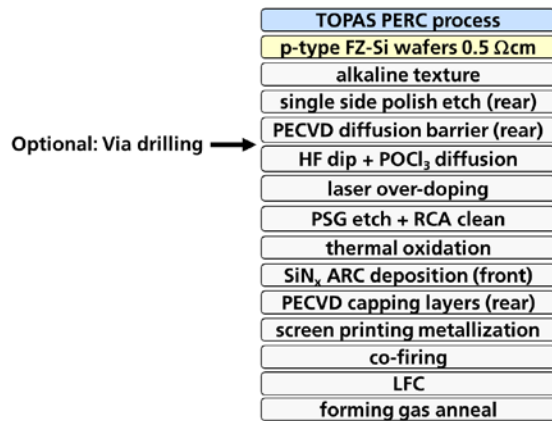


Fig. 2: Process flow for the fabrication of PERC solar cells using the TOPAS approach.

2.2 Fabrication of p-type MWT-PERC solar cells

Again, boron-doped FZ-Si wafers with a base resistivity of $0.5 \Omega\text{cm}$ and a thickness of $200 \mu\text{m}$ are used. However, the fabrication of MWT-PERC solar cells follows a slightly different fabrication sequence. Fig. 3 a) illustrates the process flow. We apply a single side texture and diffusion, using a thermal oxide barrier layer. Of course, for manufacturing purposes, other approaches would be chosen for realising emitters on only one side of the sample, e.g. deposited diffusion barriers, single side emitter removal, directional emitter formation by deposited dopant sources or ion implantation [12-14], and first results will be shown also in this paper.

The emitter on the front surface is again passivated by a thin SiO_2 layer grown in O_2 ambient. A small adaption of the fabrication process results in either a device with rear emitter underneath the solder contacts (in the following denoted as MWT-PERC, see Fig. 3 b) or a structure without rear emitter (denoted as high performance MWT, HIP-MWT [6], see Fig. 3 c). Apart from that, the same processes as for the PERC solar cells are applied.

As the HIP-MWT structure does not require a structured rear side, fabrication of these cells is significantly simplified compared to the MWT-PERC

structure with rear emitter, which makes this structure suitable for industrial manufacturing.

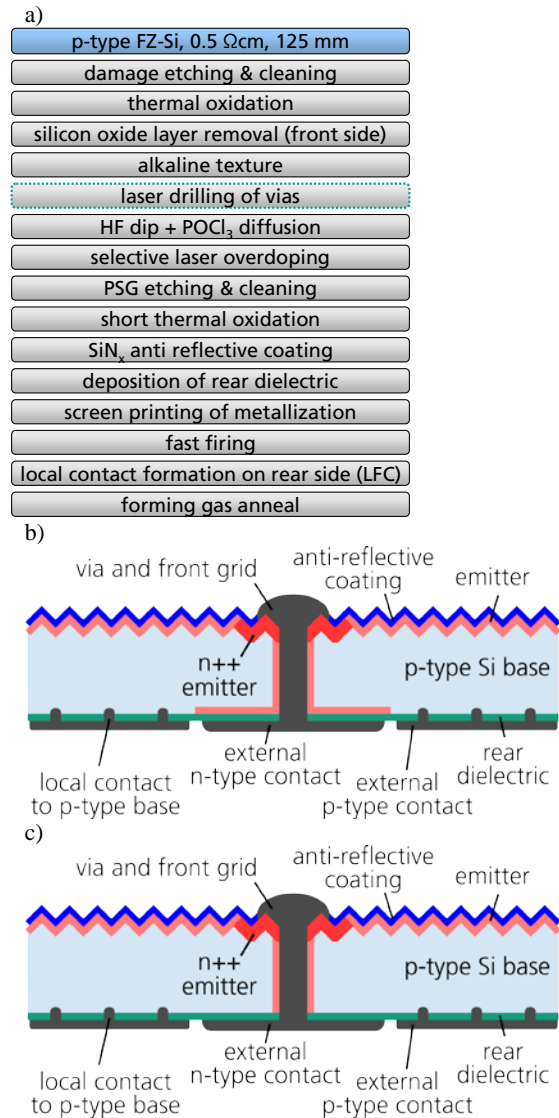


Fig. 3: a) Process flow for the fabrication of MWT-PERC solar cells. b) Schematic cross section of the used MWT-PERC structure with rear emitter. c) Schematic cross section of the used HIP-MWT [6] structure without rear emitter.

Please note that the drilling of vias with an infrared laser is the only process step required to combine MWT and PERC into HIP-MWT structures.

Apart from the process flow illustrated in Fig. 3 a), we also apply via drilling for the first time on one small group of samples fabricated with the process flow of Fig. 2 to fabricate HIP-MWT solar cells. All other processes are identical. This further simplifies the fabrication sequence for highly-efficient HIP-MWT solar cells.

3 RESULTS

3.1 PERC solar cells

Table I lists the current-voltage (I/V) parameters of the best p-type FZ-Si PERC solar cells fabricated within this project. The open circuit voltage of 661 mV underlines the high quality front and rear surface passivation of the

thermal oxide layers. The selective emitter ensures a low specific contact resistance of around $\rho_c = 3 \text{ m}\Omega\text{cm}^2$. A fill factor $FF = 78.9\%$ and a conversion efficiency $\eta = 20.0\%$ are achieved [15]. The stability of the applied process sequence shows in a very narrow distribution, with a median conversion efficiency of 19.9% . Applying the same processes, conversion efficiencies of 19.8% have been achieved on 156 mm sized cast-mono Si wafers [16].

Table I: Cell parameters measured after processing using an industrial cell tester. All solar cells have a total cell area of 149 cm^2 .

*Calibrated measurement at Fraunhofer ISE CalLab PVCells

	V_{oc} (mV)	J_{sc} (mA/cm^2)	FF (%)	ρFF (%)	η (%)
PERC <i>best cell</i>	661	38.3	78.9	83.6	20.0*
median (8)	662	38.5	78.2	83.4	19.9

3.2 MWT-PERC solar cells

Table II lists the IV parameters of the best fabricated p-type MWT solar cells with four different structures: MWT-PERC with rear emitter (see Fig. 3 b), HIP-MWT without rear emitter (see Fig. 3 c) and a structure denoted HIP-MWT+, which is an even further simplified structure without via emitter [17]. Also listed is a HIP-MWT solar cell fabricated with the process flow shown in Fig. 2 with additional via drilling (last row, denoted HIP-MWT*). The MWT-PERC solar cells feature a thick thermal oxide layer on the rear, whereas for the HIP-MWT and HIP-MWT+ solar cell, a thin thermal oxide layer is used. Furthermore, in Table II also two different technologies for silver front contact formation are listed, namely screen printing (SP) and dispensing (D). Please note that the solar cells were fabricated in different experiments. A MWT chuck [18] developed at Fraunhofer ISE allows for accurately measuring the IV parameters either in an industrial cell tester or at Fraunhofer ISE CalLab PVCells.

Table II: IV parameters of the best solar cells measured after processing using an industrial cell tester. A custom-made chuck allows for the measurement of the MWT cells. The measurement on Cz-Si is performed after annealing of the B-O-complex (annealed) or after light induced degradation by illumination at > 0.2 suns for 36 h (after LID). Please note the different cell structures MWT-PERC (with rear emitter), HIP-MWT (without rear emitter) and HIP-MWT+ (simplified HIP-MWT structure without via emitter). All solar cells have a total cell area of 149 cm^2 . Front contact metallization: screen printed (SP), dispensed (D). Base resistivity $0.5 \Omega\text{cm}$ (FZ), $1.8 \Omega\text{cm}$ (Cz).

* Calibrated measurement at Fraunhofer ISE CalLab PVCells

** HIP-MWT with single side polishing and only one thermal oxidation process (see Fig. 2).

		η (%)	V_{oc} (mV)	J_{sc} (mA/cm^2)	FF (%)	Ref.
MWT-PERC	SP (FZ)	20.1*	658	39.0	78.4	[6]
HIP-MWT	SP (FZ)	20.2*	664	39.5	77.1	[6]
HIP-MWT+	SP (FZ)	20.3*	664	39.2	78.1	[19]
	D (FZ)	20.6*	661	39.9	78.3	[20]
	D (Cz, annealed)	20.1*	651	40.3	76.6	[20]
MWT-PERC	D (Cz, after LID)	19.7*	645	40.1	76.1	[20]
HIP-MWT**	SP (FZ)	20.1	660	39.0	78.2	-

As apparent from the first three rows in Table II, the combination of rear surface passivation (PERC, high V_{oc}) and reduced shading (MWT, high J_{sc}) results in screen printed solar cells with conversion efficiencies exceeding 20% , with a peak efficiency of 20.3% for the most simplified structure HIP-MWT+, which underlines the high efficiency potential of these devices.

All solder contacts of MWT solar cells are formed by screen printing technology. As a result, there is no strain on the front contacts during soldering, which reduces the requirements for front contact adhesion and promotes the use of very thin silver fingers. On some solar cells, dispensing technology is used as an alternative technology to screen printing for front contact formation.

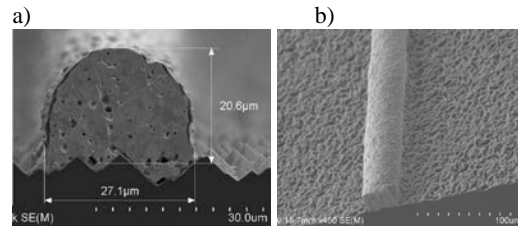


Fig. 4: Scanning electron microscope image showing the a) cross section and b) top view of two dispensed silver contact fingers with an aspect ratio of up to 0.86.

The scanning electron microscope picture in Fig. 4 a) shows a cross section of a dispensed silver finger with a width of $27 \mu\text{m}$ and an aspect ratio of 0.76, here on Cz-Si with an alkaline texture. Apart from the low finger width, which leads to low shading values, also the semi-circle shaped geometry is noteworthy, which enables low specific contact resistance values and sufficient adhesion, as well as effective reflection of incoming photons to the wafer surface. Moreover, this finger is fabricated by multi-nozzle dispensing of 10 fingers in parallel, highlighting the progress achieved recently in this promising technology [21].

The bird's eye view of another dispensed Ag finger [21] with $34 \mu\text{m}$ width and $29 \mu\text{m}$ height (aspect ratio of 0.86) on iso-textured surface in Fig. 4 b), for which a different Ag paste and a single nozzle system is used, indicates a very homogeneous cross-section and furthermore no variations in the finger height.

As expected from the scanning electron microscope images, a first implementation of dispensed silver fingers in MWT-PERC solar cells results in an increase of J_{sc} by $0.7 \text{ mA}/\text{cm}^2$ due to reduced shading, see Table II, which increases the conversion efficiency up to 20.6% [20]. The application of dispensed silver fingers on Cz-Si wafers results in a peak efficiency of 20.1% in the annealed state (after annealing of the boron oxygen complex) and 19.7% in the degraded state. Please note that the actual finger cross section is different to the newer results shown in Fig. 4, due to the use of a not optimized silver paste, which results in increased specific contact resistance values [22].

A calculation based on realistic assumptions of certain process improvements reveals that with MWT-PERC-type structures stable conversion efficiencies beyond 21% are possible [22]; a value that seems reasonable, regarding publications of other companies on PERC solar cells with conversion efficiencies of 21% [23].

Merging the MWT with the TOPAS sequence (thin SiO_2 layer on rear) in this first experiment also allows for

conversion efficiencies beyond 20% (HIP-MWT**) as listed in Table II, which strongly streamlines the fabrication sequence. The median as well as the maximum conversion efficiency of 7 cells is 20.1%, the increase of $\Delta\eta = 0.1-0.2\%_{\text{abs}}$ compared to the results of Table I results from a higher J_{sc} due to reduced shading. Again, only via drilling as additional process makes the full benefit of reduced shading accessible. As no further experiments have been conducted, we expect process improvements to raise this value even further.

4 MODULE ASSEMBLY

To prove the industrial feasibility of the cell structures developed within the project, some demonstrator modules have been fabricated. All solar cells are fabricated from 0.5 Ωcm FZ-Si and feature a selective emitter, thermal oxide passivated surfaces and screen-printed contacts. Due to the low number of solar cells available, the modules consist of only a limited number of cells.

Contacting of the solar cells in the PERC module is realised by using standard cell interconnectors on front and rear in case of the PERC module and by structured interconnectors for reduced mechanical stress [24] in case of the HIP-MWT module. These first experiments form the basis for a potentially easier module integration of MWT cells. Table III shows the results of *IV* measurements, for the solar cells at an industrial cell tester and for the module at Fraunhofer ISE CalLab PV Modules under standard test conditions (STC) using a rectangular mask with a spacing of 1 mm to the wafer edge.

The two cell PERC module achieves an open-circuit voltage of $V_{\text{oc}} = 1320$ mV and a conversion efficiency of $\eta = 17.7\%$, whereas for the one cell MWT module $V_{\text{oc}} = 657$ mV and $\eta = 18.2\%$ are extracted. Please also note the low cell to module loss of the *FF* for the MWT-PERC module of only 1.4% absolute, which results from the possible use of structured cell interconnectors with a larger cross-section, which leads to a low series resistance.

Higher module efficiencies are possible by the use of full-square Si wafers, due to the more efficient use of available module space; however this has not been implemented in this project.

Several other companies report on progress in module assembly of p-type MWT solar cells [1, 25], with a peak power of 289 W_p .

Table III: *IV* parameters of cells measured after processing using an industrial cell tester and after module encapsulation at Fraunhofer ISE CalLab PV Modules using a rectangular symmetric element. The symmetric element has a spacing of 1 mm to the wafer edge. The pseudo-square cells fabricated of 0.5 Ωcm FZ-Si are of 125 mm dimension and feature silver contacts realized by single-step screen printing.

Category		Area (cm^2)	η (%)	V_{oc} (mV)	<i>FF</i> (%)	$\Delta FF_{\text{cell-module}}$ (% _{abs})
PERC	Cells	148.6	19.9	662	78.2	-
	module	322.6	17.7	1320	75.9	2.3
MWT- PERC	Cell	148.6	20.1	656	78.5	-
	module	161.3	18.2	657	77.1	1.4

5 SUMMARY

This paper summarises the results of the MASSE project, which targeted the development of 20% efficient p-type crystalline silicon solar cells. Several novel technologies have been deployed for reaching this goal. A selective emitter by laser-overdoping increases J_{sc} and V_{oc} , compared to homogeneous emitters. A thermal oxidation step is used to improve the emitter profile and to simultaneously passivate both phosphorous emitter and rear p-type base. Laser fired contact technology forms the local rear contacts through the rear dielectric layers, followed by inline annealing in forming gas for reduced recombination. An application of these technologies results in PERC devices with a conversion efficiency of 20.0%.

As the use of these technologies is not limited to PERC structures, MWT structures have been implemented in the following. The elimination of the external front busbar contacts increases J_{sc} , further reduction of shading is achieved by dispensed silver contact fingers with high aspect ratios. Process evolution allows omitting the rear emitter in MWT-PERC structures, which eliminates the need for masking and structuring steps. A further developed structure, called HIP-MWT+ even overcomes the need for a via emitter, which makes this structure perfectly suited for industrial manufacturing, as only one additional process step, namely via drilling, makes the full benefit of reduced shading accessible. With this approach, on high-quality FZ-Si peak efficiencies of 20.3% have been achieved with screen printed silver contacts and 20.6% with dispensed silver contacts. A first experiment with a streamlined process sequence already yields a conversion efficiency of 20.1%.

Fabricated demonstrator modules show a low cell to module loss of the *FF*, and conversion efficiencies of 17.7% for the PERC module and 18.2% for the MWT-PERC module.

Apart from dispensing technology, high-capacity equipment for all technologies is commercially available. The strong focal point on processes with industrial cycle times in this project calls for a fast transfer of these cell structures into industrial manufacturing.

6 ACKNOWLEDGMENTS

We gratefully acknowledge the technical support by the PV-TEC co-workers. This work was funded by the German Federal Ministry for the Environment, Nature Conservation and Nuclear Safety (Contract numbers 0329849B and 0325404).

REFERENCES

- [1] Y. Gassenbauer, *et al.*, IEEE Journal of Photovoltaics **3** (2012), p. 125-130.
- [2] K. A. Münzer, *et al.*, Proceedings of the 27th European Photovoltaic Solar Energy Conference and Exhibition (2012), p. 666-671.
- [3] T. Dullweber, *et al.*, Proceedings of the 27th European Photovoltaic Solar Energy Conference and Exhibition (2012), p. 672-675.

- [4] J. W. Müller, *et al.*, Proceedings of the 27th European Photovoltaic Solar Energy Conference and Exhibition (2012), p. 661-665.
- [5] E. van Kerschaver, *et al.*, Proceedings of the 2nd World Conference on Photovoltaic Energy Conversion (1998), p. 1479-1482.
- [6] B. Thaidigsmann, *et al.*, Physica Status Solidi RRL **5** (2011), p. 286-288.
- [7] S. Mack, *et al.*, Proceedings of the 35th IEEE Photovoltaic Specialists Conference (2010), p. 17-21.
- [8] K. R. McIntosh and L. P. Johnson, Journal of Applied Physics **105** (2009), p. 124520.
- [9] M. J. Kerr and A. Cuevas, Semiconductor Science and Technology **17** (2002), p. 35-38.
- [10] E. Schneiderlöchner, *et al.*, Progress in Photovoltaics: Research and Applications **10** (2002), p. 29-34.
- [11] S. Mack, *et al.*, Proceedings of the 26th European Photovoltaic Solar Energy Conference and Exhibition (2011), p. 1089-1093.
- [12] J.-H. Lai, *et al.*, IEEE Journal of Photovoltaics **1** (2011), p. 16-21.
- [13] H. Hieslmaier, *et al.*, Energy Procedia **27** (2012), p. 122-128.
- [14] S. Mack, *et al.*, Proceedings of the 27th European Photovoltaic Solar Energy Conference and Exhibition (2012), p. 875-878.
- [15] U. Jäger, *et al.*, IEEE Journal of Photovoltaics **3** (2013), p. 621-627.
- [16] C. Schwab, *et al.*, Energy Procedia **40** (2013), p. 611-617.
- [17] B. Thaidigsmann, *et al.*, presented at *this conference* (2013).
- [18] M. Glatthaar, *et al.*, Proceedings of the 25th European Photovoltaic Solar Energy Conference and Exhibition (2010), p. 2118-2120.
- [19] E. Lohmüller, *et al.*, Proceedings of the 27th European Photovoltaic Solar Energy Conference and Exhibition (2012), p. 590-595.
- [20] E. Lohmüller, *et al.*, IEEE Electron Device Letters **32** (2011), p. 1719-1721.
- [21] M. Pospischil, *et al.*, presented at *39th IEEE PVSC* (2013).
- [22] B. Thaidigsmann, *et al.*, Solar Energy Materials and Solar Cells **106** (2012), p. 89-94.
- [23] A. Lachowicz, *et al.*, Proceedings of the 27th European Photovoltaic Solar Energy Conference and Exhibition (2012), p. 1846-1850.
- [24] U. Eitner, D. Eberlein, and M. Tranzitz, Proceedings of the 27th European Photovoltaic Solar Energy Conference and Exhibition (2012), p. 3461-3464.
- [25] Y. Weiwei, *et al.*, IEEE Journal of Photovoltaics **3** (2013), p. 697-701.